energies

MDPI

Article

A Fault Diagnosis Method of the Shearer Hydraulic Heightening System Based on a Rough Set and RBF Neural Network

Min Liu [1,2,*], Zhiqi Liu [2], Jinyuan Cui [3] and Yigang Kong [2]

[1] College of Intelligent Manufacturing Engineering, Shanxi Institute of Science and Technology, Jincheng 048000, China
[2] College of Mechanical Engineering, Taiyuan University of Science and Technology, Taiyuan 030024, China
[3] College of Mechanical and Vehicle Engineering, Taiyuan University of Technology, Taiyuan 030024, China
* Correspondence: liumin@sxist.edu.cn

Abstract: The hydraulic heightening system is the core component of the shearer, and its stable operation directly affects the safety and reliability of the equipment, so it is of great significance to realize an efficient and accurate fault diagnosis. This paper proposes a fault diagnosis method combining a rough set and radial basis function neural network (RS-RBFNN). Firstly, the RS is used to discretize the original fault data set and attribute reduction, remove the redundant information, and mine the implicit knowledge and potential rules. Then, the topology structure of the RBFNN is determined. The mapping relationship is established between the fault symptom and category. The fault diagnosis is carried out with Python language. Finally, the method is compared with two diagnostic methods including a back propagation neural network (BPNN) and RBFNN. The research results show that the RS-RBFNN has the highest fault diagnosis accuracy, with an average of 98.68%, which verifies the effectiveness of the proposed fault diagnosis method.

Keywords: hydraulic heightening system; fault diagnosis; RS-RBFNN; simulation; accuracy

Citation: Liu, M.; Liu, Z.; Cui, J.; Kong, Y. A Fault Diagnosis Method of the Shearer Hydraulic Heightening System Based on a Rough Set and RBF Neural Network. *Energies* **2023**, *16*, 956. https://doi.org/10.3390/en16020956

Academic Editor: Helena M. Ramos

Received: 7 December 2022
Revised: 10 January 2023
Accepted: 12 January 2023
Published: 14 January 2023

1. Introduction

The shearer is one of most the important pieces of equipment to realize the mechanization and modernization of coal mine production. It is mainly composed of a cutting part, loading part, walking part, and hydraulic elevation system [1,2]. In longwall mining faces, the cutting part breaks down the coal from the coal body and loads it into the mining machine of the working conveyor, with a complex system and harsh working environment [3]. Its stable operation is directly related to the safety and stability of coal mining. Once failure occurs, it causes huge economic losses and hidden dangers of safety production. As the key component of the shearer, the failure rate of the hydraulic heightening system accounts for about 12% of the total failure, and the duration accounts for about 40% of the average time of failure. The causes of failure are diverse and uncertain [4]. When the traditional identification method is used for fault diagnosis, a large amount of redundant data is obtained, which leads to low efficiency and poor accuracy of fault diagnosis [5]. Therefore, it is of great significance to establish an efficient and accurate fault diagnosis method for the hydraulic heightening system of the shearer.

Generally speaking, the failure of the hydraulic heightening system mainly occurs in the leakage and mechanical failure of hydraulic pumps, valves, and cylinders [6]. At present, experts and scholars have various methods for the fault diagnosis of hydraulic systems and internal components. Reference [7] proposed a deep learning model method based on the combination of a convolutional neural network and long- and short-term memory, which improves the accuracy of the hydraulic system fault diagnosis by improving the ability of data extraction. Article [8] proposed a new FDI framework for the closed-loop system

to diagnose the faults of the hydraulic system, which mainly constructs the performance residual vector for diagnosis and compares the difference between the real and model system stability, accuracy, and speed. In [9], a fault diagnosis information fusion method of the hydraulic system based on the improved D-S evidence theory and time–space domain was proposed, which uses D-S and decision rules to identify faults. Reference [10] proposed a fault feature extraction method for hydraulic systems based on a fuzzy ARX model, which has the advantage of extracting nonlinear features for fault classification and diagnoses. Reference [11] proposed a two-stage radial basis function neural network model for fault classification detection and the fault location of the hydraulic system. In [12], a scheme combining a regression neural network and metric learning was proposed. Degradation features are extracted from the difference between the actual and estimated outputs to diagnose the faults of the hydraulic system. Reference [13] optimized the placement and method of sensors in the hydraulic system, improved the efficiency of data acquisition, and realized the efficient fault diagnosis of the hydraulic system. Reference [14] proposed an adaptive particle swarm optimization algorithm to optimize the BP neural network method. By using a particle purity better than the optimal value and the dynamic fusion strategy to realize the particle swarm search, the hydraulic system diagnosis efficiency was improved. Reference [15] proposed a new fault diagnosis method which could extract leakage information, directly detect and locate faults in the hydraulic system caused by leakage, and realize intuitive and efficient fault monitoring. In reference [16], based on the machine learning algorithm and statistical features of vibration monitoring, a C4.5 decision tree algorithm was adopted to extract statistical features from vibration signals to realize the fault diagnosis of the hydraulic system.

Aiming at the fault diagnosis of hydraulic systems, the fault features of the hydraulic pump, valve, and cylinder were extracted for fault diagnosis. Reference [17] used a cavitation detection framework, including experimental research and numerical signal processing, to detect the strength of cavitation faults in axial piston pumps, so as to improve the accuracy of fault diagnosis. Reference [18] improved the identification accuracy and optimized the parameters of the hydraulic plunker pump through the improved LeNet-5 and PSO hyperparameter optimization fault diagnoses. In [19], a three-layer fault diagnosis method based on the Dezert–Smarandache theory was used. A multi-classifier was used to detect the failure of the hydraulic system with the hydraulic valve as the main object. Reference [20] applied diagnostic methods based on wavelet packet analysis and feature extraction. By optimizing the identification and extraction of the fault features, the hydraulic cylinder leakage of the actuator in the hydraulic system was diagnosed.

There are a variety of state-of-art methods based on deep neural networks. In [21], a multi-scale edge-labeling graph neural-network-based method was developed under small samples, which take advantage of a graph neural network in the feature extraction of small samples and improved its performance through a multi-scale trick. Reference [22] proposed a novel entropy-based sparsity measure for the prognosis and development of a sparsogram to select a sensitive filtering band. The measurements were sensitive to pulses and could indicate how sparse the signal was. A sparsogram tool was developed to help choose the right filtering band for envelope analysis. Reference [23] proposed a fault diagnosis method based on an RBFNN. A series of fault isolation observers based on an RBFNN were designed to completely decouple different faults. The diagnosis results of one component were not affected by other faults, and multiple faults could be diagnosed at the same time. In [24], a hybrid fault diagnosis method was developed based on relief, a principal component analysis (PCA), and a deep neural network. Relief and PCA were used to select fault features to reduce data dimensions, and deep neural networks were used to improve the accuracy of fault diagnosis. In [25], based on the laboratory measurement data of the GEROLER motor, the black box model for predicting the operating parameters of the artificial neural network was established. By comparing the static multilayer feedforward network and dynamic NARX neural network, the dynamic NARX neural network provided better results due to its flexibility in processing non-linear dynamic systems. The above

fault diagnosis methods are diverse, but there are few fault diagnosis methods for hydraulic systems based on an RS-RBFNN.

Through the analysis of the existing hydraulic system fault diagnosis methods, it can be seen that the diagnosis data is complicated and the diagnosis method is single, resulting in low diagnosis efficiency and accuracy. This paper presents a fault diagnosis method of the shearer hydraulic heightening system based on an RS-RBFNN. First, the RS was used to discretize the dataset and attribute reduction, which removed redundant information and retained the key features of the data [26]. It laid a data foundation for subsequent feature extraction, shortened the training time of the network, and significantly improved the efficiency. Then, the RBFNN had a strong input and output mapping function, with only the best approximation characteristics. Combined with the better association and memory ability of the RBFNN, the hidden knowledge was mined and the potential rules were objectively described [27,28]. Therefore, aiming at the problems of fault data redundancy and the complex mutual relationship of shearer hydraulic heightening systems, compared with the existing single method, the combination method of an RS and RBFNN not only takes advantage of RS data processing, but also combines the best local approximation performance and global optimal characteristics of the RBFNN to achieve a faster and more accurate fault diagnosis.

The organization of this paper is as follows: Section 2 mainly introduces the RS-RBFNN fault diagnosis model and methods. Section 3 is the fault simulation analysis of the hydraulic heightening system. Section 4 presents the process of fault diagnosis with the RS-RBFNN. Section 5 is the comparison of the three fault diagnosis methods. Finally, Section 6 draws the conclusion.

2. Models and Methods

Figure 1 shows the whole idea of the RS-RBFNN fault diagnosis method. It mainly included five parts: model building, fault data collection, RS preprocessing (includes cutting the clutter and attribute reduction), RBFNN training diagnosis, and fault output.

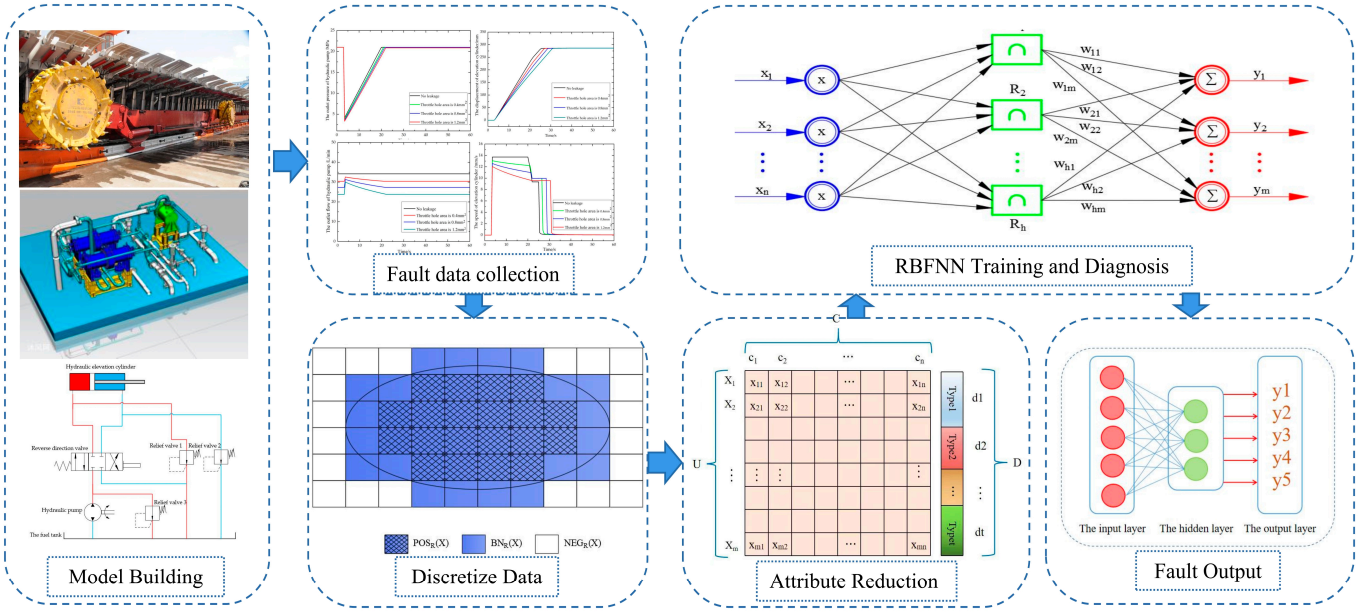

Figure 1. The whole idea of the RS-RBFNN fault diagnosis method.

2.1. RS Model

Data plays an important role in artificial intelligence. In order to solve complex problems, large amounts of data are often needed and structures are established to process them. An RS is also based on a large amount of data, building models for discretization and attribute reduction [27,29].

The data system used was represented by $S = (U, A, V, f)$ where U is the domain and A is the set of attributes, both of which are non-empty finite sets; $V = UV_a$ where V_a is the attribute range; and $f : U \times A \to V$ is the value of an object's property, $a \in A$, $f(x, a) \in V_a$.

Data systems are usually represented by relational tables. As a special information system, decision tables play a key role in decision applications. The row attribute represented our research object, and the column attribute represented the object attribute.

In the data system S, $A = C \cup D, C \cap D = \varnothing$, C represented the set of conditional attributes and D represented the set of decision attributes. If the data system contained a set of C and D, the system was a decision table.

Assume an equivalence relation cluster L on U, $P \subseteq L$, $P \neq \varnothing$, $\cap P$ is an equivalence relation in U, defined as an indistinguishable relation on P, expressed as:

$$ind(P) : [x]_{ind(P)} = \bigcap_{L \in P} [x]_L \tag{1}$$

The indistinguishable relationship divides U into multiple sets, in which the objects are indistinguishable. $U/ind(P)$ is the knowledge related to all equivalence classes of $ind(P)$ in the domain. $K = (U, S)$ is called the basic set of P in U, recorded as U/P. The equivalence class of $ind(P)$ is the basic category of knowledge P. If T is called the T-elementary knowledge about U, the equivalence class of T is called the T-elementary category of R. There is the knowledge base $K = (U, R)$, for each subset $x \subseteq U$ and $R \in ind(K)$, the R lower approximation set and the R upper approximation set of X are defined as follows:

$$\underline{R}X = \cup\{Y \in U/R | Y \subseteq X\} \tag{2}$$

$$\overline{R}X = \cup\{Y \in U/R | Y \cap X \neq \varnothing\} \tag{3}$$

The R boundary region of X is defined as $BN_R(X) = \overline{R}X - \underline{R}X$; the R-positive region of X is defined as $POS_R(X) = \underline{R}X$. The R-negative domain of X is defined as $NEG_R(X) = U - \overline{R}X$. It can be concluded that $\overline{R}X = POS_R(X) \cup BN_R(X)$.

The set is approximated by the exact sets $\underline{R}X$ and $\overline{R}X$. All objects of $POS_R(X)$ belong to X. The object of the negative domain $NEG_R(X)$ must not belong to X, and the object of the boundary domain $BN_R(X)$ is not sure whether it belongs to X.

If $Q \subseteq P$, then Q is independent and if ind *(Q) = ind(P)*, then Q is a reduction of P. The reduction of the decision table does not affect the original knowledge expression after removing the redundant conditional attributes.

2.2. RBFNN Model

Figure 2 shows the topology structure of the RBFNN used in this study. The RBFNN is a kind of feedforward network, where the number of nodes in the input, hidden, and output layers are n, h, and m, respectively. The input vector of the network is $x = [x_1, x_2, \ldots, x_n]^T \in R^n$, the weight matrix is $W \in R^{h \times m}$, and the output vector is $Y = [y_1, y_2, \ldots, y_m]^T$. The activation function of the hidden layer neurons is R_i in the network, and the $\sum$ represents the function of the output that is linear in the output layer.

In the network structure, the basis functions of the hidden layer are radial basis functions as activation functions, which are radially symmetric [30]. The most commonly used Gauss function can be expressed as follows:

$$R_i(x) = \exp(-\frac{||x - c_i||^2}{2\sigma_i^2}), i = 1, 2, \ldots, p \tag{4}$$

where c_i is the center of the ith basis function; σ_i is the variance of the ith basis function; and $R_i(x)$ is the hidden layer activation function corresponding to the input x_i.

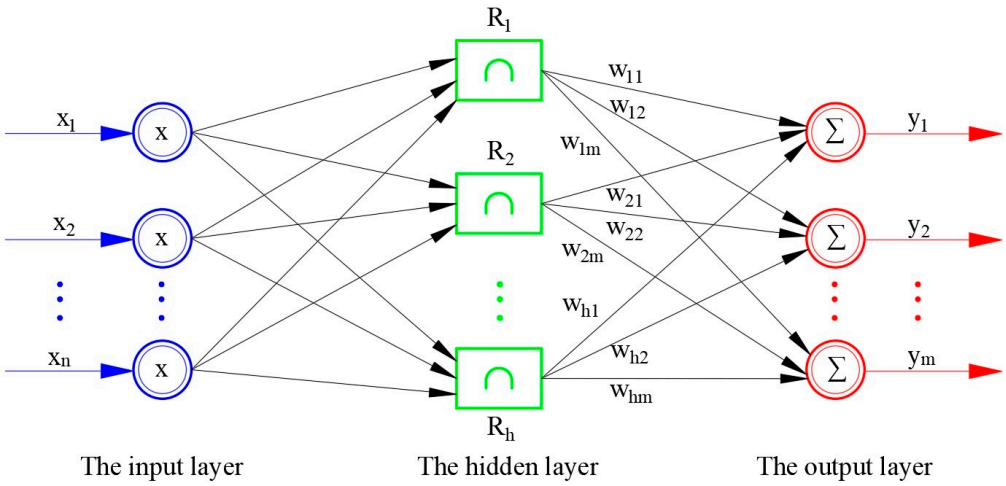

Figure 2. The topology structure of the RBFNN.

The input and hidden layers of the network have a nonlinear relationship, and the hidden and output layers have a linear relationship [31]. The output of the network is as follows:

$$y_k = \sum_{i=1}^{p} \omega_{ki} R_i(x), k = 1, 2, \ldots, q \tag{5}$$

where ω_{ki} is the adjustment weight between the output and hidden layers and q is the number of output layer nodes.

2.3. RS-RBFNN Fault Diagnosis Model

Figure 3 shows the flow chart of fault diagnosis model based on the RS-RBFNN. The specific flow is as follows.

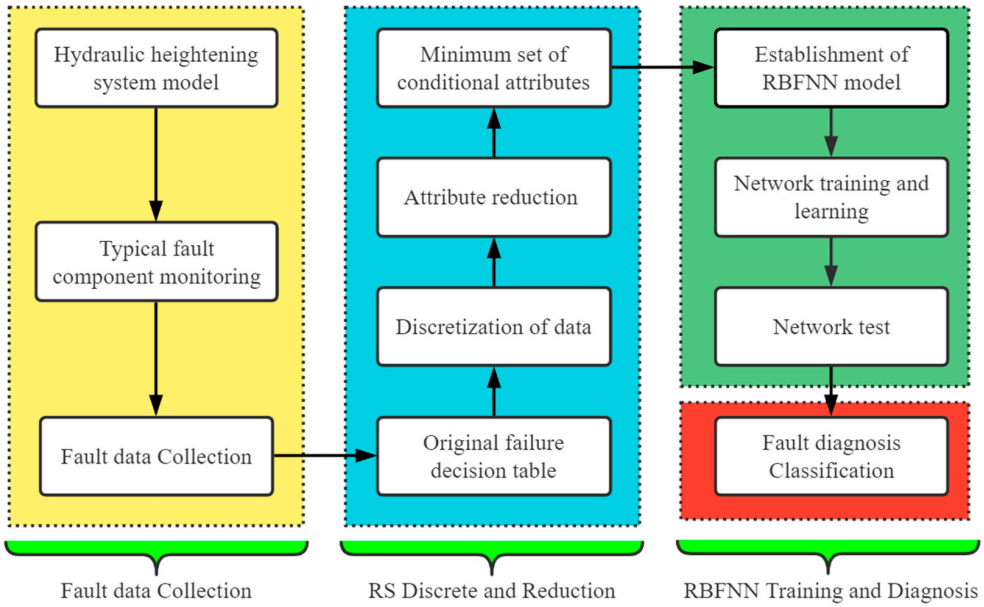

Figure 3. The flow chart of fault diagnosis model based on the RS-RBFNN.

- The model of the hydraulic heightening system was established, and the typical faults in the system were taken as the research object. Pressure, flow, displacement, and speed sensors were used to collect the fault data.
- RS theory was used to construct the original fault decision table. The fault symptoms that occurred many times in the system were taken as the condition attributes, and the

fault type was taken as the decision attribute to generate the original fault decision table. The data of the original fault decision table was discretized at an equal distance. Then, using the attribute reduction based on genetic algorithm, the redundant conditional attributes were deleted under the condition of retaining the key input information, and the minimum set of conditional attributes was obtained.

- The minimum attribute reduction set was used as the input of the RBFNN. The mapping relationship between the fault symptoms and categories of the RBF neural network was used for learning and training. Finally, the fault diagnosis classification results of the shearer hydraulic heightening system were obtained.

3. Simulation

3.1. Research Object

In this paper, the hydraulic heightening system of an MG750/1940-WD AC traction shearer used in the actual production of a coal mine was taken as the research object to model and analyze. The hydraulic heightening system includes a hydraulic cylinder, hydraulic pump, three-bit four-way reversing valve, relief valve, etc. Figure 4 shows the schematic diagram of the hydraulic heightening system. In the schematic diagram, the red line represents "the high pressure flow channel", and the blue line represents "the low pressure flow channel".

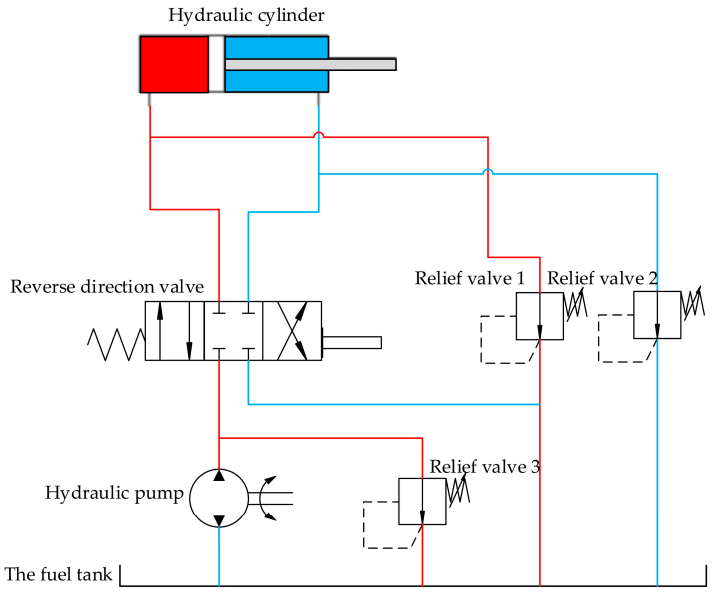

Figure 4. The schematic diagram of the hydraulic heightening system.

3.2. Simulation Model

According to the actual working parameters, the simulation model of the hydraulic heightening system was established using Matlab R2018b/SimHydraulics software, which was highly close to the actual production. Table 1 shows the main parameters of the model.

Table 1. The main parameters of the model.

Category	Parameter
Hydraulic pump pressure	21 MPa
Hydraulic pump speed	188 rad/s
Hydraulic pump displacement	3.675×10^{-6} m^3/rad
Valve core opening amount	5×10^{-3} m
Leakage area	1×10^{-12} m^2
Cylinder piston rod displacement	490 mm
Hydraulic cylinder rodless cavity area	4.15×10^{-2} m^2
Hydraulic cylinder rod cavity area	2.82×10^{-2} m^2

Figure 5 shows the simulation model of the hydraulic heightening system. To monitor the operating status of the system, multiple sensors were set up to detect the hydraulic pump pressure and flow, actuator speed, displacement, etc. The locations of the pressure, flow, displacement, and velocity measurement points are indicated in the fault simulation model diagram. In the simulation model, the brown line represents "hydraulic pipeline", the dark green line represents "mechanical structure connection", and the light green line represents "electric and hydraulic power source".

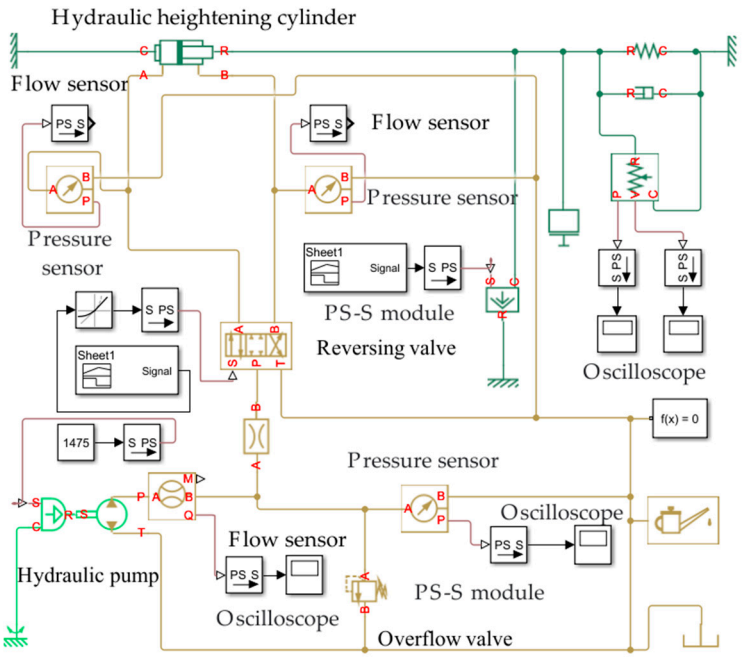

Figure 5. The simulation model of the hydraulic heightening system.

In the hydraulic heightening system, the most frequently occurring faults in actual production were selected as typical faults for analysis, including hydraulic pump internal leakage, the reversing valve being stuck, and the external leakage of the hydraulic cylinder. In the established simulation model, the fault conditions were simulated and datasets were collected. Firstly, the hydraulic pump was connected in parallel with a throttle hole. By adjusting the flow rate of the throttle hole, the simulation of different internal leakages of the hydraulic pump was realized. Then, by setting different displacement openings of the directional valve, the jamming condition of the directional valve was simulated. Last, the external leakage of the hydraulic cylinder was caused by a gap between the piston rod and hydraulic cylinder cover, so the external leakage was simulated by adding an external orifice.

When the internal leakage occurred in the hydraulic pump, Figure 6 shows the outlet flow of the hydraulic pump, the outlet pressure of the hydraulic pump, and the speed and the displacement curve of the hydraulic cylinder. When the internal leakage occurred in the hydraulic pump, the outlet flow stability value and outlet pressure of the pump decreased. With the serious leakage of the hydraulic pump, the rotation speed of the cylinder piston rod decreased, and the extension time of the cylinder piston rod became longer.

When the reversing valve failed, Figure 7 shows the pressure of the rod chamber and the speed of the hydraulic cylinder curve. With the decrease of the opening of the reversing valve, the response time of the system gradually increased, and the running speed of the piston rod decreased.

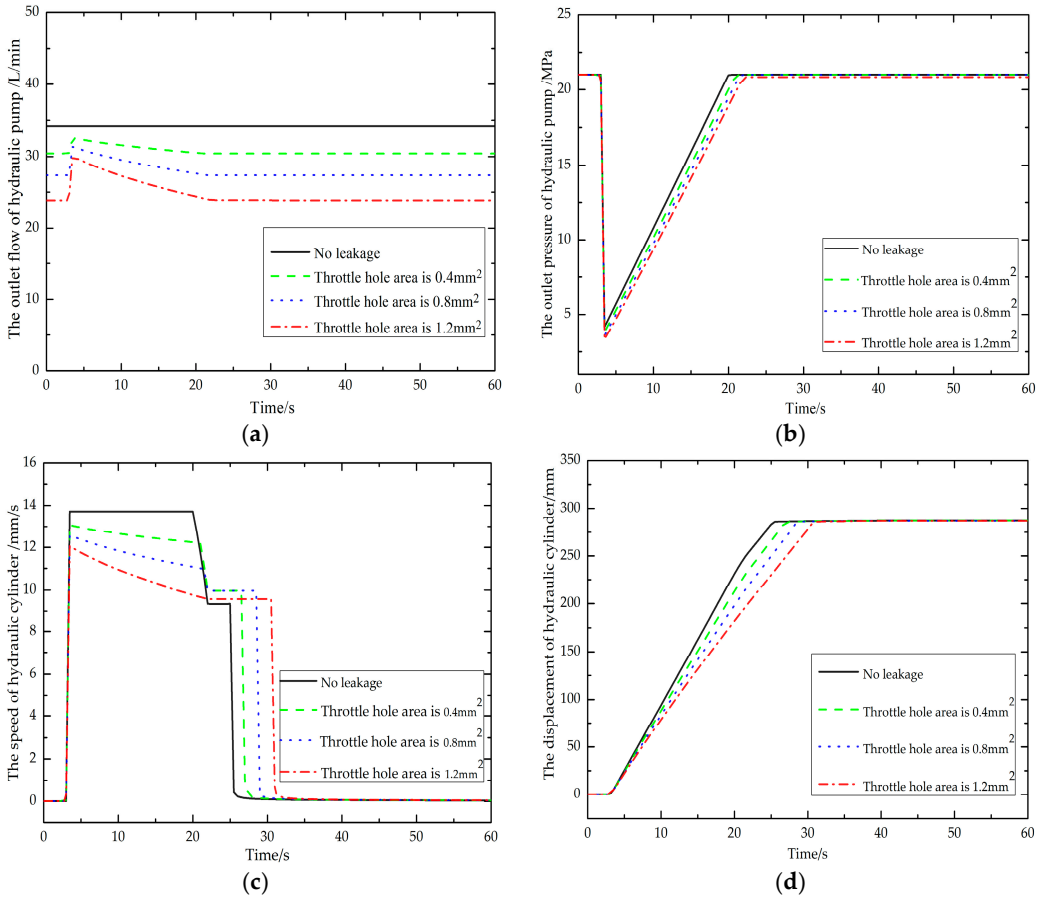

Figure 6. When the internal leakage occurred in the hydraulic pump. (**a**) The outlet flow of the hydraulic pump; (**b**) the outlet pressure of the hydraulic pump; (**c**) the speed of the hydraulic cylinder; (**d**) the displacement of the hydraulic cylinder.

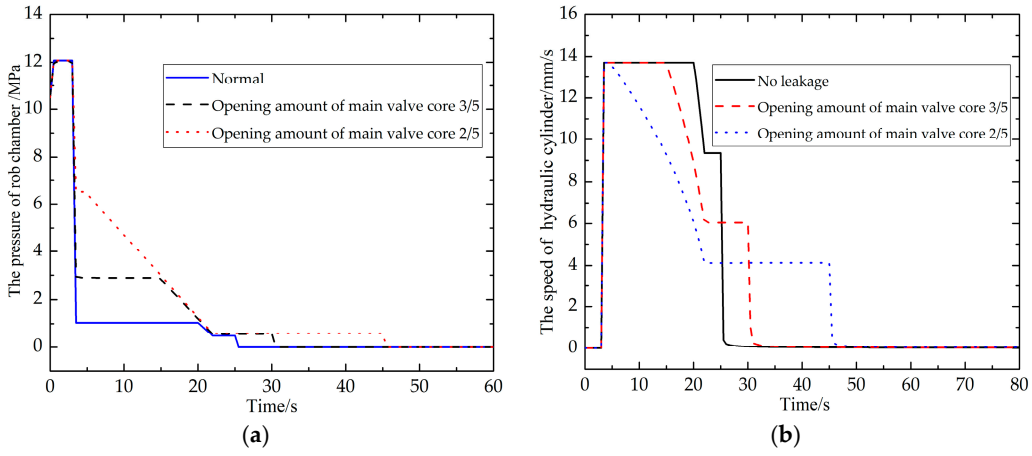

Figure 7. When the reversing valve failed. (**a**) The pressure of the rod chamber; (**b**) the speed of the hydraulic cylinder.

When the hydraulic cylinder was exposed to external leakage, Figure 8 shows the pressure of the rodless chamber and the displacement of the hydraulic cylinder. The pressure gradually decreased in the rodless chamber of the hydraulic cylinder, and the time required became longer for the piston rod of the hydraulic cylinder to reach the maximum stroke. Since the given flow of the system was larger than the flow required by the rocker arm movement, the hydraulic cylinder could still complete the work when the leakage was

small. But the external leakage had a serious impact on the accuracy and stability of the hydraulic heightening system to reach the specified position.

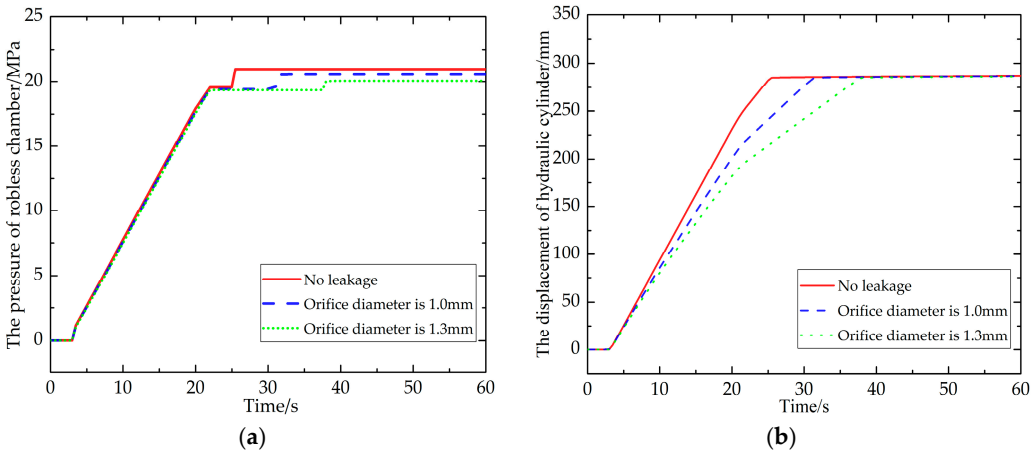

Figure 8. When the hydraulic cylinder was exposed to external leakage. (**a**) The pressure of the rodless chamber; (**b**) the displacement of the hydraulic cylinder.

4. Results of Fault Diagnosis

4.1. RS Preprocessing

An RS was used to preprocess the typical fault data of the hydraulic heightening system. Based on the typical faults of hydraulic heightening systems, 510 groups of fault data samples were selected to establish an original fault decision table.

Table 2 is the original fault decision table. The set C of fault symptoms was used as the condition attribute $C = \{C_1, C_2, \ldots C_{11}\}$. It represented the working condition of the shearer, the speed of the hydraulic cylinder, the displacement of the hydraulic cylinder, the outlet flow of the hydraulic pump, the inlet flow of the hydraulic pump, the outlet pressure of the hydraulic pump, the inlet pressure of the hydraulic pump, the inlet flow of the hydraulic cylinder, the outlet flow of the hydraulic cylinder, the pressure of the rodless chamber, and the pressure of the rod chamber, respectively. The fault category served as the decision attribute D, $D = \{0, 1, 2, 3, 4\}$. These represented the normal system, the slight leakage of the hydraulic pump, the serious leakage of the hydraulic pump, the jamming of the reversing valve, and the external leakage of the hydraulic cylinder of five typical conditions, respectively.

Table 2. The original fault decision table.

Sample	Condition Attribute									Decision Attribute D
	C_1	C_2 (mm/s)	C_3 (mm)	C_4 (L/min)	C_5 (L/min)	C_6(kPa)	…	C_{10} (kPa)	C_{11} (kPa)	
1	0	0.00	0.00	34.17	34.17	21,003.89	…	10,501.95	10,501.95	0
2	0	0.00	0.00	34.17	34.17	21,003.89	…	8203.76	12,071.76	1
…	…	…	…	…	…	…	…	…	…	…
260	1	11.99	65.61	29.88	29.88	8307.38	…	5975.21	796.04	2
261	2	11.94	71.59	29.76	29.76	8786.80	…	6473.89	789.43	3
…	…	…	…	…	…	…	…	…	…	…
510	1	13.08	4.40	34.17	34.17	4106.27	…	1052.44	949.01	4

C1 in Table 2 represents the shearer's working condition, "0" represents the shearer's initial working condition, and the shearer parameters remained constant in C1. The number "1" represents the starting condition of the shearer when the roller reached the specified height and the traction speed reached the normal speed from "0"; "2" indicates the normal working condition of the shearer, and the height and traction speed of the drum reached the rated value and remained unchanged.

The set C of fault symptoms and five decision attributes constituted the original data matrix, which constituted the decision system domain U.

The continuous attributes of data samples were discretized and normalized as follows:

$$x' = \frac{x - Z_{\min}}{Z_{\max} - Z_{\min}} \tag{6}$$

where $Z_{\min}$ and $Z_{\max}$ represent the minimum and maximum values in data C, respectively, and x' represents the processed data.

Physical quantities, such as pressure and flow rates, are continuous values in the original fault decision table. Because it did not meet the processing conditions of rough sets, it needed to be discretized. The normalized decision table was processed by the equal distance discretization method. The range of attributes was divided into five parts and represented by the corresponding numbers: zero, one, two, three, and four.

The reduction algorithm based on the genetic algorithm was used for reduction. Using the mathematical toolkit ROSETTA based on the RS theoretical framework, the minimum conditional attribute set obtained was eight, which was $\{C_1, C_2, C_3, C_4, C_6, C_8, C_{10}, C_{11}\}$. The minimum conditional attribute set corresponded to the discretized decision table data, and then the minimum decision table was obtained by deleting repeated rows, as shown in Table 3.

Table 3. The minimum decision table.

Sample	Condition Attribute								Decision Attribute D
	C_1	C_2	C_3	C_4	C_6	C_8	C_{10}	C_{11}	
1	0	1	1	4	4	1	2	4	0
2	1	4	1	4	1	4	1	2	0
…	…	…	…	…	…	…	…	…	…
260	0	1	1	4	4	1	2	4	2
261	1	4	1	4	2	4	1	3	2
…	…	…	…	…	…	…	…	…	…
510	2	1	4	4	4	1	4	1	4

Based on RS theory, the data was well-mined and reduced in scale and quantity, and the core knowledge in the data was obtained, which laid the foundation for the subsequent diagnosis.

4.2. RBFNN Diagnosis

The minimal condition attribute set after RS reduction was taken as the input of the RBFNN, $x = [x_1, x_2, x_3, x_4, x_5, x_6, x_7, x_8]^T$. The x values were the normal working condition of the system, the speed of the hydraulic cylinder, the displacement of the hydraulic cylinder, the outlet flow of the hydraulic pump, the outlet pressure of the hydraulic pump, the inlet flow of the hydraulic cylinder, the pressure of the hydraulic cylinder with the rodless chamber, and the pressure of the hydraulic cylinder with the rod chamber, respectively. The number of neural nodes in the network input layer was eight. The fault category was used as the output, $y = [y_1, y_2, y_3, y_4, y_5]$. The y values represented no fault, slight leakage fault of the hydraulic pump, serious leakage fault of the hydraulic pump, stuck fault, and hydraulic cylinder leakage fault, respectively. The number of neural nodes in the network output layer was five. According to the network training results, the number of hidden layer neurons was eleven with fast convergence. Figure 9 shows the topology structure of the RS-RBFNN.

According to the topology structure of the RBFNN, 450 groups of samples were selected as training samples, and 60 groups of samples were selected as test samples for training and testing. The parameters of the RBFNN function were initialized by Python programming language, including the center and width of the hidden layer and the weight

from the hidden layer to the output layer. Table 4 shows the training sample, and Table 5 shows the test sample.

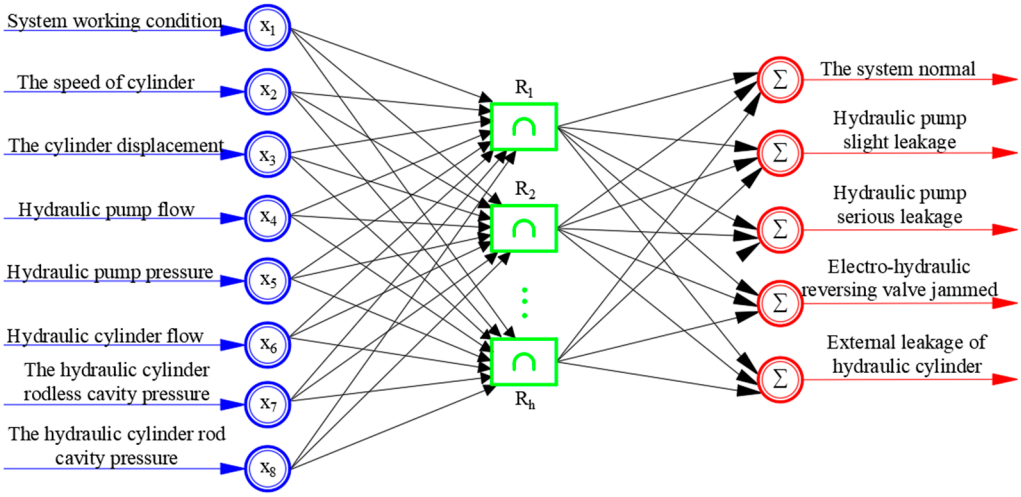

Figure 9. The topology structure of the RS-RBFNN.

Table 4. The training sample.

Training Sample	x_1	x_2	x_3	x_4	x_5	x_6	x_7	x_8	y
1	0.50	1.00	0.02	1.00	0.06	1.00	0.05	0.09	0
2	0.50	1.00	0.04	1.00	0.08	1.00	0.08	0.09	0
3	1.00	0.73	0.77	0.44	1.00	0.73	0.92	0.05	1
...	...	...	...	...	...	...	...	...	...
447	0.50	0.86	0.01	0.61	0.00	0.86	0.04	0.06	2
448	1.00	0.44	0.82	1.00	1.00	0.44	0.94	0.05	3
449	0.50	0.61	0.75	1.00	1.00	0.81	0.91	0.03	4
450	1.00	0.00	1.00	1.00	1.00	0.21	0.99	0.00	4

Table 5. The test sample.

Test Sample	x_1	x_2	x_3	x_4	x_5	x_6	x_7	x_8
1	1.0	0.68	0.97	1.00	1.00	0.68	0.93	0.04
2	1.0	0.73	0.85	0.44	1.00	0.73	0.92	0.05
3	1.0	0.00	1.00	0.00	1.00	0.00	1.00	0.00
4	1.0	0.44	0.87	1.00	1.00	0.44	0.94	0.05
...	...	...	...	...	...	...	...	...
60	0.5	0.95	0.02	1.00	0.05	1.00	0.05	0.08

The RBFNN used the gradient descent method as the learning algorithm of the network. In Python programs, the distance between the feature sample and the RBF mean value was calculated, and the output of the hidden layer, input, and output of the output layer were calculated. The maximum number of iterations of the RBFNN was set to 5000, the learning rate η = 0.1, and the training error target value was 0.001. Figure 10 shows the RS-RBFNN training error curve.

The results showed that the RS-RBFNN fault diagnosis method was used to diagnose the typical faults of the hydraulic heightening system, which had high diagnostic accuracy and a fast network convergence speed. The average diagnostic accuracy reached 98.68%. When the training step was 47, the network tended to be stable and the learning speed was fast, which can meet the technical requirements of the system in practical applications.

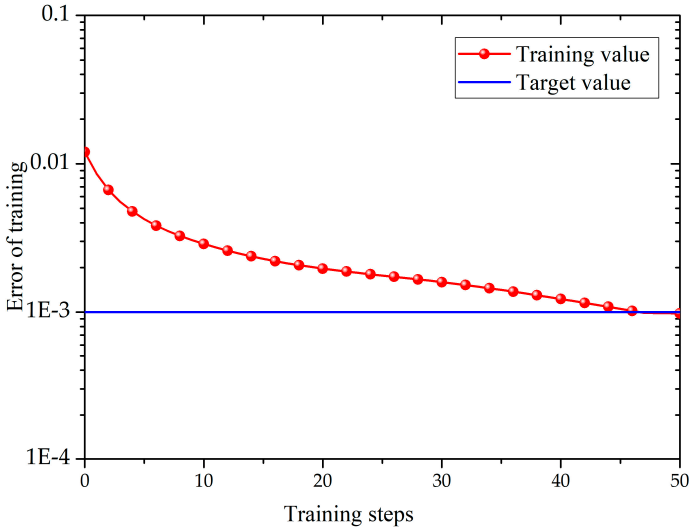

Figure 10. The RS-RBFNN training error curve.

5. Simulation Comparison

To further verify the effectiveness of the proposed method, a variety of simulation methods were compared. Two other mainstream fault diagnosis schemes are introduced: BPNN and RBFNN.

The BPNN diagnosis method is the most traditional neural network diagnosis method, which belongs to a nonlinear forward network. The main idea of diagnosis is to input data samples and use a back-propagation algorithm to adjust the weights and deviations of the network so that the output vector is as close as possible to the expected vector. When the error square sum of the network output layer is less than the specified error, the diagnosis method training is completed [32,33]. However, the network connection mode is "weight connection", and the convergence speed is slow. A BPNN is trained and tested by using the original fault decision table.

RBFNN diagnostic methods, similar to those of a BPNN as described above, are a class of commonly used three-layer feedforward networks that can be used for both function approximation and pattern classification. They have the best approximation performance and global optimal characteristics, and the training speed is fast. An RBFNN uses the original fault decision table to train and test the network.

The RS-RBFNN diagnosis method is based on RBFNN diagnosis. Using an RS to reduce the original fault decision table, the minimum condition attribute set is obtained for training. The number of hidden nodes of the network is the optimal number of nodes according to multiple simulations. Table 6 shows the comparison parameter of the three neural network simulations.

Table 6. The comparison parameter of the three neural network simulations.

Parameter	BPNN	RBFNN	RS-RBFNN
Fault data sample	510	510	510
Number of iterations	5000	5000	5000
Learning rate	0.1	0.1	0.1
Error target value	0.001	0.001	0.001
Output layer	Sigmoid	Gaussian	Gaussian
Network structure	11-14-5	11-14-5	8-11-5

The diagnostic results of the three typical fault diagnosis methods were obtained with a simulation comparison, as shown in Figure 11. The RS-RBFNN diagnosis method had the best fault diagnosis performance, and its average diagnostic accuracy can reach 98.68%. The diagnostic effect of an RBFNN was lower than that of an RS-RBFNN, and the average

diagnostic accuracy was 92.59%. A BPNN had the worst diagnostic effect, and its average diagnostic accuracy was only 83.09%.

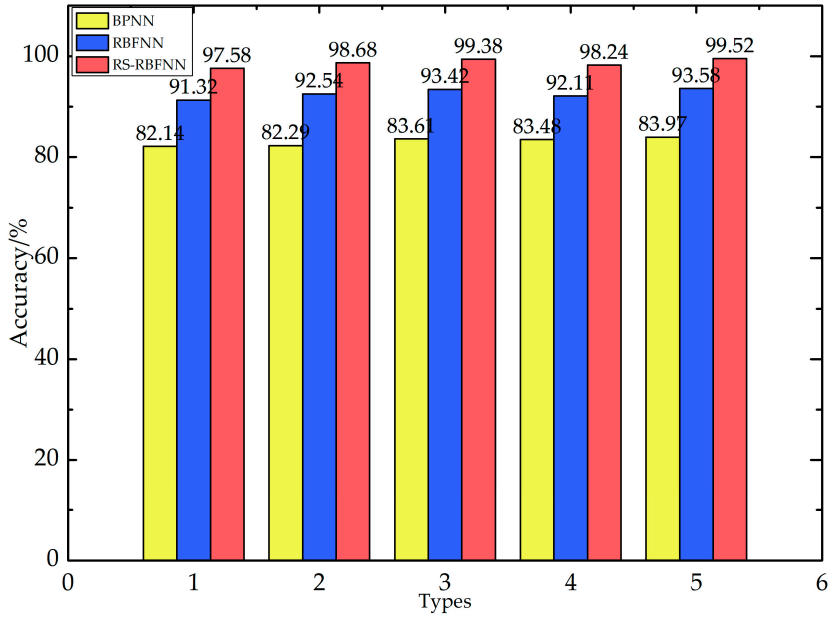

Figure 11. The accuracy comparison of the three fault diagnosis methods.

6. Conclusions

Aiming at the requirements of high efficiency and high precision for the fault diagnosis of hydraulic heightening systems, this paper proposes a fault diagnosis method based on an RS-RBFNN. The original fault data was extracted by establishing the shearer hydraulic heightening system model. The ability of RS theory was utilized to process redundant data, including discretizing processing and attribute reduction, which provided better data input for fault diagnosis. The mapping relationship between the fault symptoms and fault categories of the RBF neural network was used for learning and training. The average accuracy of the final diagnosis result was 98.68%.

To verify the accuracy of the proposed method, two other mainstream fault diagnosis schemes were introduced for comparison: the BPNN and RBFNN methods. The results showed that the RS-RBFNN diagnosis method had the best fault diagnosis performance, and its average diagnostic accuracy could reach 98.68%, which was higher than that of the RBFNN by about 6.09%, and higher than that of the BPNN by 15.59%.

For the shearer hydraulic heightening system, the method was proved to be effective. In the future, this method can be extended to the fault diagnosis of hydraulic systems of various machines, including excavators, cranes, forklifts, and heavy trucks.

Author Contributions: Conceptualization, M.L. and Z.L.; methodology, M.L. and Y.K.; software, J.C.; validation, M.L., Z.L. and J.C.; formal analysis, Y.K.; investigation, Z.L.; resources, Y.K.; data curation, Z.L.; writing—original draft preparation, M.L. and J.C.; writing—review and editing, M.L.; supervision, Y.K. All authors have read and agreed to the published version of the manuscript.

Funding: This research was funded by the National Natural Science Foundation of China (project number 51975396) and the Shanxi Institute of Science and Technology Project (project number XKY015).

Data Availability Statement: The data used to support the findings of this study are available from the first author upon request.

Acknowledgments: We would like to express our great thanks to the editors and reviewers for their helpful suggestions to improve the quality of this paper.

Conflicts of Interest: The authors declare no conflict of interest.

References

1. Ma, X.; Wang, G. Fault Monitoring System of Shearer Based on DSP. *Appl. Mech. Mater.* **2014**, *9*, 973–976.
2. Zhang, X.; Yao, G.; Zhang, Y. Nonlinear multi body dynamic modeling and vibration analysis of a double drum coal shearer. *J. Cent. South Univ.* **2021**, *28*, 2120–2130. [CrossRef]
3. Li, X.; Tang, R.; Sha, Y.; Bai, S.; Zhang, J. Fault Diagnosis Expert System of Continuous Miner Hydraulic System. *Adv. Mat. Res.* **2012**, *619*, 463–466.
4. Bołoz, Ł.; Rak, Z.; Stasica, J. Comparative Analysis of the Failure Rates of Shearer and Plow Systems—A Case Study. *Energies* **2022**, *15*, 6170. [CrossRef]
5. Gao, F.; Xiao, L.; Zhong, W.; Liu, W. Fault Diagnosis of Shearer Based on Fuzzy Inference. *Appl. Mech. Mater.* **2011**, *1229*, 1577–1580.
6. Li, S.; Yang, Z.; Tian, H.; Chen, C.; Zhu, Y.; Deng, F.; Lu, S. Failure Analysis for Hydraulic System of Heavy-Duty Machine Tool with Incomplete Failure Data. *Appl. Sci.* **2021**, *11*, 1249. [CrossRef]
7. Yang, J. Research on Fault Diagnosis of Shearer Hydraulic System Based on Information Fusion Technology. Master's Thesis, North University of China, Taiyuan, China, 2021.
8. Zhang, Y.; Wang, S.; Shi, J.; Yang, X.; Zhang, J.; Wang, X. SAR performance-based fault diagnosis for electrohydraulic control system: A novel FDI framework for closed-loop system. *Chin. J. Aeronaut.* **2022**, *35*, 381–392. [CrossRef]
9. Dong, Z.; Zhang, X. Modified D-S evidential theory in hydraulic system fault diagnosis. *Procedia Environ. Sci.* **2011**, *11*, 98–102.
10. He, X. Fault diagnosis approach of hydraulic system using FARX model. *Procedia Eng.* **2011**, *15*, 949–953. [CrossRef]
11. Liu, H.; Wang, S.; Ouyang, P. Fault Diagnosis in a Hydraulic Position Servo System Using RBF Neural Network. *Chin. J. Aeronaut.* **2006**, *19*, 346–353. [CrossRef]
12. Song, D.; Lu, C.; Ma, J.; Cheng, Y. Health Assessment for Hydraulic System based on GRNN and Metric Learning. *IFAC PapersOnline* **2020**, *53*, 37–42. [CrossRef]
13. Kong, X.; Cai, B.; Liu, Y.; Zhu, H.; Liu, Y.; Shao, H.; Yang, C.; Li, H.; Mo, T. Optimal sensor placement methodology of hydraulic control system for fault diagnosis. *Mech. Syst. Sig. Process.* **2022**, *174*, 109069. [CrossRef]
14. Wang, R.; Sun, W. Fault diagnosis of electrical automatic control system of hydraulic support based on particle swarm optimization algorithm. *J. Ambient Intell. Hum. Comput.* **2022**, *4*, 22–29. [CrossRef]
15. Fu, X.; Liu, B.; Zhang, Y.; Lian, L. Fault diagnosis of hydraulic system in large forging hydraulic press. *Measurement* **2014**, *49*, 390–396. [CrossRef]
16. Jegadeeshwaran, R.; Sugumaran, V. Comparative study of decision tree classififier and best fifirst tree classififier for fault diagnosis of automobile hydraulic brake system using statistical features. *Measurement* **2013**, *46*, 3247–3260. [CrossRef]
17. Lan, Y.; Li, Z.; Liu, S.; Huang, J.; Niu, L.; Xiong, X.; Niu, C.; Wu, B.; Zhou, X.; Yan, J.; et al. Experimental investigation on cavitation and cavitation detection of axial piston pump based on MLP-Mixer. *Measurement* **2022**, *200*, 111582. [CrossRef]
18. Zhu, Y.; Li, G.; Wang, R.; Tang, S.; Su, H.; Cao, K. Intelligent fault diagnosis of hydraulic piston pump combining improved LeNet-5 and PSO hyperparameter optimization. *Appl. Acoust.* **2021**, *183*, 108336. [CrossRef]
19. Ji, X.; Ren, Y.; Tang, H.; Xiang, J. DSmT-based three-layer method using multi-classififier to detect faults in hydraulic systems. *Mech. Syst. Sig. Process.* **2021**, *153*, 107513. [CrossRef]
20. Zhao, X.; Zhang, S.; Zhou, C.; Hu, Z.; Li, R.; Jiang, J. Experimental study of hydraulic cylinder leakage and fault feature extraction based on wavelet packet analysis. *Comput. Fluids.* **2015**, *106*, 33–40. [CrossRef]
21. Zhou, Y.; Zhi, G.; Chen, W.; Qian, Q.; He, D.; Sun, B.; Sun, W. A new tool wear condition monitoring method based on deep learning under small samples. *Measurement* **2022**, *189*, 110622. [CrossRef]
22. Zhou, Y.; Kumar, A.; Parkash, C.; Vashishtha, G.; Tang, H.; Xiang, J. A novel entropy-based sparsity measure for prognosis of bearing defects and development of a sparsogram to select sensitive filtering band of an axial piston pump. *Measurement* **2022**, *203*, 111997. [CrossRef]
23. Guo, X.; Tian, M.; Li, Q.; KiAhn, C.; Yang, Y. Multiple-fault diagnosis for spacecraft attitude control systems using RBFNN-based observers. *Aerosp. Sci. Technol.* **2020**, *106*, 106195. [CrossRef]
24. Wen, X.; Xu, Z. Wind turbine fault diagnosis based on ReliefF-PCA and DNN. *Expert Syst. Appl.* **2021**, *178*, 115016. [CrossRef]
25. Gregov, G. Modeling and predictive analysis of the hydraulic GEROLER motor based on artificial neural network. *Eng. Rev.* **2022**, *42*, 91–100. [CrossRef]
26. Qiu, Z.; Min, R.; Wang, D.; Fan, S. Energy features fusion based hydraulic cylinder seal wear and internal leakage fault diagnosis method. *Measurement* **2022**, *195*, 111042. [CrossRef]
27. Zhang, D.; Zhu, P. Variable radius neighborhood rough sets and attribute reduction. *Int. J. Approx. Reason.* **2022**, *150*, 98–121. [CrossRef]
28. Yakovyna, V.; Shakhovska, N. Software failure time series prediction with RBF, GRNN, and LSTM neural networks. *Procedia Comput. Sci.* **2022**, *207*, 837–847. [CrossRef]
29. Yuan, Z.; Chen, H.; Li, T.; Yu, Z.; Sang, B.; Luo, C. Unsupervised attribute reduction for mixed data based on fuzzy rough sets. *Inf. Sci.* **2021**, *572*, 67–87. [CrossRef]
30. Xiang, B.; Mu, Q. Gimbal control of inertially stabilized platform for airborne remote sensing system based on adaptive RBFNN feedback model. *IFAC J. Syst. Control.* **2021**, *16*, 100148. [CrossRef]

31. Zeng, X.; Zhen, Z.; He, J.; Han, L. A feature selection approach based on sensitivity of RBFNNs. *Neurocomputing* **2018**, *275*, 2200–2208. [CrossRef]
32. Li, J.; Yao, X.; Wang, X.; Yu, Q.; Zhang, Y. Multiscale local features learning based on BP neural network for rolling bearing intelligent fault diagnosis. *Measurement* **2020**, *153*, 107419. [CrossRef]
33. Wang, C.; Kang, Y.; Shen, P.; Chang, Y.; Chung, Y. Applications of fault diagnosis in rotating machinery by using time series analysis with neural network. *Expert Syst. Appl.* **2010**, *37*, 1696–1702. [CrossRef]